Scientia Iranica F (2013) 20(6), 2297–2305

Sharif University of Technology
Scientia Iranica
Transaction F: Nanotechnology
www.scientiairanica.com

Study of nanofluid natural convection in an inclined L-shaped cavity

A.A. Abbasian Arani[a*], A.Z. Maghsoudi[a], A.H. Niroumand[a] and S.M.E. Derakhshani[b]

a. *Department of Mechanical Engineering, University of Kashan, Kashan, P.O. Box 87317-51167, Iran.*
b. *Department of Mechanical Engineering, Jasb Center Branch, Islamic Azad University, Delijan, Iran.*

Received 31 July 2012; received in revised form 23 December 2012; accepted 6 May 2013

KEYWORDS
L-shaped cavity;
Natural convection;
Nanofluid;
Finite volume method.

Abstract. This study has focused on natural convection in an inclined L-shaped cavity filled with copper-water nanofluid. The governing equations including continuity, momentum and energy equations have been discretized with a control volume method (FVM) using the SIMPLER algorithm. A proper upwinding scheme is employed to obtain stabilized solutions. The effective parameters are solid volume fraction ($0, \leq \varphi \leq 0.05$), inclination angle ($0^\circ \leq \gamma \leq 135^\circ$), shape factor ($0.6 \leq 2W/L \leq 1$) and Rayleigh number ($10^1 \leq Ra \leq 10^5$). Results have been presented as isotherm lines, stream lines, local Nusselt number and average Nusselt number. The effects of Rayleigh number, inclination angle and shape factor, as well as the solid volume fraction, have been investigated on the flow field and Nusselt number. Results show that the solid volume fraction and shape factor, as well as the inclination angle, have important effects on the flow field, especially on average Nusselt number. The results indicate that a decrease in shape factor and an increase in solid volume fraction lead to an increase in average Nusselt number.

1. Introduction

Natural convection in enclosures has a wide range of applications in engineering technologies, such as solar thermal receivers, energy-saving household refrigerators, electronic cooling, double-wall thermal insulation, and etc. In recent years, natural convection inside irregular and complex shaped enclosures, such as arc-shaped enclosures [1], wavy enclosures [2], enclosures with irregular walls [3] and eccentric elliptical enclosures [4], have attracted attention in engineering applications. The problem of convection heat transfer in L-shaped enclosures has been extensively studied because of its wide applications in such as electronic packages, electrical equipment, building corners, etc. [5]. Most previous work investigated natural convection in enclosures filled with ordinary fluids, such as air, water, etc. The most important problem of these fluids is their low thermal conductivities. An innovative way to overcome this problem is to utilize special fluids that are a mixture of nanoparticles and base fluid. These fluids are named nanofluids, and are created by dispersing nanometer-sized particles (< 100 nm) in a base fluid such as water, ethylene glycol or propylene glycol. Using metallic particles with high thermal conductivity increases the thermal conductivity of such mixtures. Eastman et al. [6], Xie et al. [7] and Jana et al. [8] showed that higher thermal conductivity can be achieved in thermal systems utilizing nanofluids. For instance, just 0.3% volume fraction of copper nanoparticles with 10 nm diameter leads to 40% increase in the thermal conductivity of ethylene glycol [9]. A brief review about the properties of nanofluids is

*. *Corresponding author: Tel.: +98 3615912413; Fax: +98 3615912424*
E-mail address: abbasian@kashanu.ac.ir (A.A. Abbasian Arani)

provided in [10,11]. The present study has focused on natural convection in L-shaped enclosures. The effective thermal conductivity of nanofluid is calculated by a model proposed by Patel [12]. To calculate the viscosity of nanofluid, a model given by Brinkman has been used [13].

2. Model and governing equations

2.1. Problem statement

In this study, natural convection in an inclined L-type cavity has been investigated. As shown in Figure 1, the left vertical and bottom horizontal walls are at a constant temperature equal to T_h (hot surfaces), and the right vertical and up horizontal walls are at a constant temperature equal to T_c (cold surfaces). Other walls are insulated. L is the length of the walls, W is the distance between internal walls, and $2W/L$ is the shape factor. T_c is equal to ambient temperature, which is considered to be 293 K, and T_h is calculated by Rayleigh number. In this study, copper-water nanofluid has been used. Table 1 presents the thermophysical properties of water and copper at the reference temperature.

The boundary conditions are shown in Figure 1. If the intersection of two hot walls is selected as the origin coordinate, the boundary conditions are as follows:

Hot walls:

$$T = T_h, \qquad u = 0, \qquad v = 0. \tag{1}$$

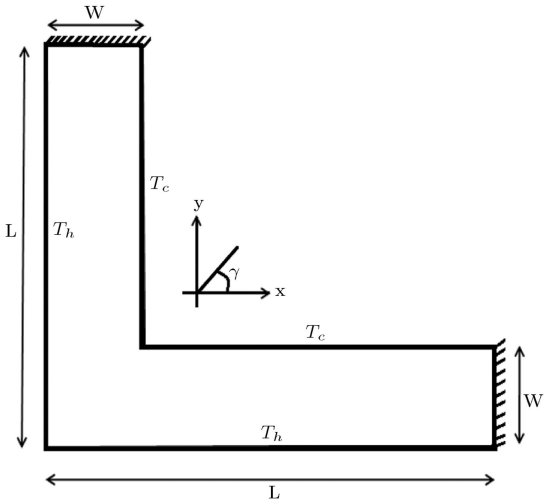

Figure 1. Problem geometry.

Cold walls:

$$T = T_c, \qquad u = 0, \qquad v = 0. \tag{2}$$

Insulated walls:

$$\frac{\partial T}{\partial n} = 0, \qquad u = 0, \qquad v = 0. \tag{3}$$

In the above relations, n is the normal unit vector on the hypothetical surface.

2.2. Governing equations

The system of governing equations, including continuity, momentum and energy equations for a steady two-dimensional laminar and incompressible flow, can be written as follows:

1. Continuity equation:

$$\frac{\partial u}{\partial x} + \frac{\partial v}{\partial y} = 0. \tag{4}$$

2. Momentum equations:

$$u\frac{\partial u}{\partial x} + v\frac{\partial u}{\partial y} = -\frac{1}{\rho_{nf}}\frac{\partial p}{\partial x} + v_{\rm nf}\nabla^2 u - \frac{g}{\rho_{\rm nf}}(T - T_c)[(1-\varphi)\rho_f\beta_f + \varphi\rho_s\beta_s]\sin\gamma, \tag{5}$$

$$u\frac{\partial v}{\partial x} + v\frac{\partial v}{\partial y} = -\frac{1}{\rho_{\rm nf}}\frac{\partial p}{\partial y} + v_{\rm nf}\nabla^2 v - \frac{g}{\rho_{\rm nf}}(T - T_c)[(1-\varphi)\rho_f\beta_f + \varphi\rho_s\beta_s]\cos\gamma. \tag{6}$$

3. Energy equation:

$$u\frac{\partial T}{\partial x} + v\frac{\partial T}{\partial y} = \alpha_{\rm nf}\left(\frac{\partial^2 T}{\partial x^2} + \frac{\partial^2 T}{\partial y^2}\right). \tag{7}$$

In the above equations, $\rho_{\rm nf}$ is the effective density of nanofluid, defined as:

$$\rho_{\rm nf} = (1-\varphi)\rho_f + \varphi\rho_s, \tag{8}$$

and φ is the solid volume fraction of nanoparticles. The thermal diffusivity of nanofluid is:

$$\alpha_{\rm nf} = \frac{k_{\rm nf}}{(\rho c_p)_{\rm nf}}. \tag{9}$$

The heat capacitance of nanofluid and the thermal expansion coefficient of nanofluid are defined as:

Table 1. Thermophysical properties of water and copper.

Property	c_p ($Jkg^{-1}K^{-1}$)	ρ (kgm^{-3})	k ($kWm^{-1}K^{-1}$)	B (K^{-1})
Water	4179	997.1	0.6	2.1×10^{-4}
Copper	383	8954	400	1.67×10^{-5}

$$(\rho c_p)_{\rm nf} = (1-\varphi)(\rho c_p)_f + \varphi(\rho c_p)_s, \tag{10}$$

$$(\rho\beta)_{\rm nf} = (1-\varphi)(\rho\beta)_f + \varphi(\rho\beta)_s. \tag{11}$$

The effective viscosity of nanofluid was introduced by Brinkman [13], as follows:

$$\mu_{\rm nf} = \frac{\mu_f}{(1-\varphi)^{2.5}}. \tag{12}$$

In Eq. (9), $k_{\rm nf}$ is the thermal conductivity of nanofluid and according to the Patel model [12] is:

$$\frac{k_{\rm eff}}{k_f} = 1 + \frac{k_p A_p}{k_f A_f} + ck_p pe\frac{A_p}{k_f A_f}, \tag{13}$$

where A_p/A_f and p_e are defined as:

$$\frac{A_p}{A_f} = \frac{d_p}{c_f}\frac{\varphi}{(1-\varphi)}, \quad p_e = \frac{u_p d_p}{\alpha_f}, \tag{14}$$

where A_p and A_f denote the heat transfer area of the nanoparticle and the molecular of the liquid, respectively, d_p is the diameter of solid particles, which, in this study, is assumed to be equal to 100 nm, and d_f is the molecular size of the liquid, taken as 2Å for water. Also, u_p is the Brownian motion velocity of nanoparticles, which is defined as:

$$u_p = \frac{2k_b T}{\pi\mu_f d_p^2}, \tag{15}$$

where k_b is the Boltzmann constant and is equal to 1.38065×10^{-23}.

Eqs. (4) to (7) can be converted to the dimensionless forms by definition of the following parameters:

$$(X,Y) = \frac{(x,y)}{L}, \qquad (U,V) = \frac{(uL,vL)}{\alpha_f}, \tag{16}$$

$$P = \frac{pL^2}{\rho_{\rm nf}\alpha_f^2}, \tag{17}$$

$$\theta = \frac{T-T_c}{T_h-T_c}, \tag{18}$$

$$P = \frac{g\beta_f \Delta T L^3}{\alpha_f v_f}. \tag{19}$$

By using the above dimensionless parameters, the governing equations are converted to dimensionless forms:

$$\frac{\partial U}{\partial X} + \frac{\partial V}{\partial Y} = 0, \tag{20}$$

$$U\frac{\partial U}{\partial X} + V\frac{\partial U}{\partial Y} = -\frac{\partial P}{\partial X} + \frac{v_{\rm nf}}{v_f}\frac{1}{\rm Re}.\nabla^2 U + {\rm Ra}\ {\rm Pr}\frac{\rho_f}{\rho_{\rm nf}}(1-\varphi+\varphi\frac{\rho_s\beta_s}{\rho_f\beta_f})\theta\sin\gamma, \tag{21}$$

$$U\frac{\partial V}{\partial X} + V\frac{\partial V}{\partial Y} = -\frac{\partial P}{\partial Y} + \frac{v_{\rm nf}}{v_f}\frac{1}{\rm Re}.\nabla^2 V + {\rm Ra}\ {\rm Pr}\frac{\rho_f}{\rho_{\rm nf}}(1-\varphi+\varphi\frac{\rho_s\beta_s}{\rho_f\beta_f})\theta\cos\gamma, \tag{22}$$

$$U\frac{\partial\theta}{\partial X} + V\frac{\partial\theta}{\partial Y} = \frac{\alpha_{\rm nf}}{\alpha_f}\left(\frac{\partial^2\theta}{\partial X^2} + \frac{\partial^2\theta}{\partial Y^2}\right). \tag{23}$$

The local Nusselt number on the hot wall surface is defined as:

$${\rm Nu}_L = \frac{k_{\rm nf}}{k_f}\frac{L}{T_h-T_c}\frac{\partial T}{\partial n}. \tag{24}$$

The average Nusselt number is calculated by integrating the local Nusselt number along the hot wall and is defined as:

$${\rm Nu}_{\rm ave} = \frac{1}{s}\int {\rm Nu}_L ds. \tag{25}$$

3. Numerical method

Solving of the governing equations is done by FVM using the SIPMLER algorithm [14]. To check the convergence of the sequential iterative solution, the sum of the absolute differences of the solution variables between two successive iterations has been calculated. Convergence is obtained when this summation falls below the convergence criterion. In this study, the convergence criterion has been chosen as 10^{-5}. In order to demonstrate the independence of the solution on the size of the grid, the solution has been undertaken for various mesh sizes.

3.1. Grid independence study

For showing grid independence of the numerical method; the solution has been undertaken for various mesh sizes. Table 2 shows the results for a test case. In this study, a uniform grid system has been used. As shown in Table 2, the values of Nusselt number for different grids are similar. The Results show that the grid system 81×81 is fine enough to obtain accurate results.

3.2. Validation of numerical code

To ensure validation of this code, flow in an L-type cavity with air as the base fluid has been investigated, and

Table 2. Results of grid independence examination.

Number of grids	Nusselt number
21×21	5.601
41×41	5.532
61×61	5.477
81×81	5.481
101×101	5.483

Table 3. Code validation, comparison of present work with a reference.

Shape factor	Grashof number	Average Nusselt number		
		Present work	Ref. [15]	Error
$2W/L = 1$	10^3	2.64	2.59	1.9
	10^4	2.84	2.95	3.7
	10^5	6.63	6.73	1.5
$2W/L = 2$	10^3	3.58	3.6	0.56
	10^4	3.66	3.62	1.1
	10^5	6.81	6.8	0.15

the results are compared with those of S. Mahmud [15]. As shown in Table 3, the maximum error is 3.7%, which is acceptable.

4. Discussion and Results

In this part, the effects of Rayleigh number and shape factor on the rate of heat transfer and the flow field are investigated. First, for different Rayleigh numbers and shape factors, the isotherm lines and stream lines are presented and, then, the effects of Rayleigh number and shape factor on local and average Nusselt number will be examined.

4.1. The velocity and temperature field

Figure 2 shows the stream lines and isotherm lines for a shape factor equal to $2W/L = 1$ and Rayleigh numbers $10, 10^4$ and 10^5 at solid volume fractions $\varphi = 0$ and 0.05. As shown in Figure 2, for low Rayleigh numbers ($\mathrm{Ra} = 10^4$), the isotherm lines developed parallel to the hot and cold walls because of their small temperature difference. This zone can be termed the conduction-dominated zone. Also, a clockwise (CW) rotating vortex is seen at the flow field distribution. This CW rotating vortex is formed because of the temperature difference between the hot and cold walls. At $\mathrm{Ra} = 10^5$, by an increase in temperature difference between the hot and cold walls, a CW rotating vortex forms between the two vertical walls, and another counter clockwise vortex between the two horizontal walls. The counter clockwise Benard cell in the horizontal part of the cavity evolves due to the hot bottom wall and cold top wall. For relatively high strength circulation in the vertical portion of the cavity, a horizontal penetration of vertical circulation occurs in the horizontal part of the cavity. This zone can be termed a convection-dominated zone. Just adjacent to the walls, these lines are parallel to the walls. This effect shows an increase in heat transfer rate. In addition, this figure shows that the solid volume fraction of nanoparticles has little effect on the flow field and temperature at low Rayleigh number. Figure 3 shows the stream lines and isotherm

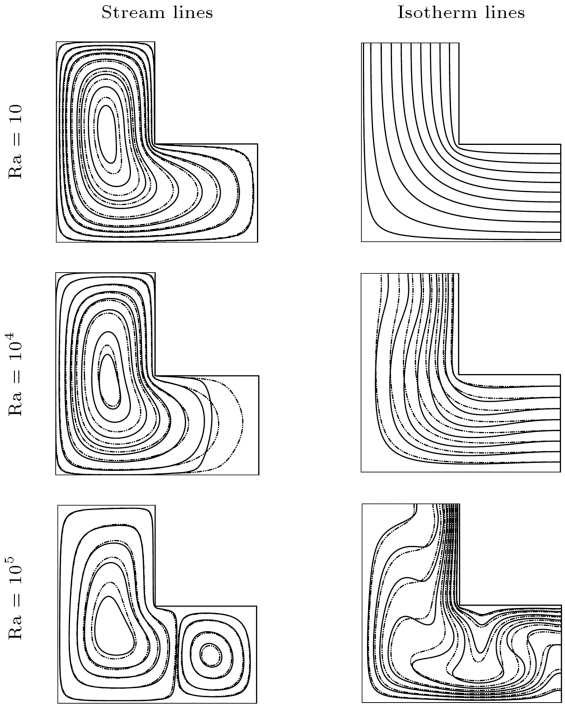

Figure 2. Isotherm lines and stream lines for $2W/L = 1$ and Rayleigh numbers $10, 10^4, 10^5$ at $\varphi = 0$ and 0.05 (the bold lines are related to pure fluid and dashed lines are related to nanofluid with $\varphi = 0.05$).

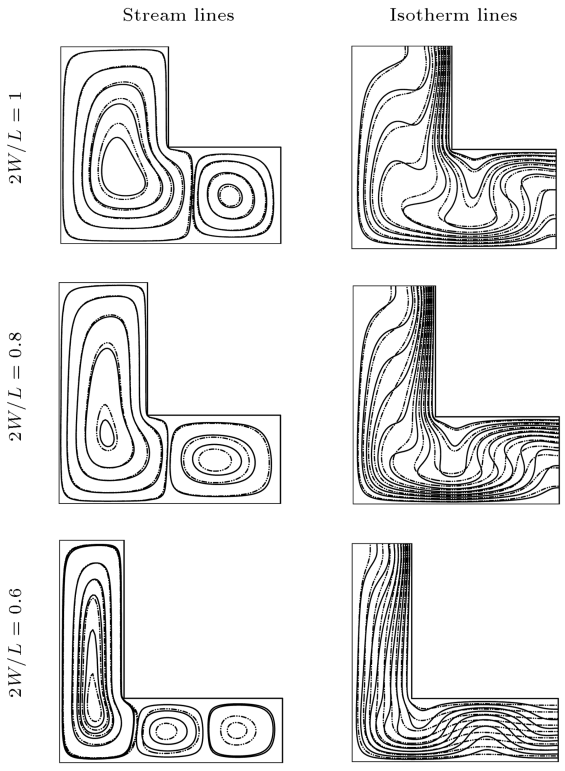

Figure 3. Isotherm lines and stream lines for $\mathrm{Ra} = 10^5$ and shape factors $2W/L = 1$, 0.8, and 0.6 (the bold lines are related to pure fluid and dashed lines are related to nanofluid with $\varphi = 0.05$).

lines for shape factors $2W/L = 0.6, 0.8$ and 1.0, and Rayleigh number Ra $= 10^5$ at $\varphi = 0$ and 0.05. As mentioned at Ra $= 10^5$, the increase in temperature difference between the hot and cold walls makes the isotherm lines just adjacent to the walls parallel to them. Also, in addition to the main CW rotating vortex, there is another rotating vortex between the two horizontal walls. However, in the case of shape factor $2W/L = 0.6$, the number of rotating vortexes increases to 2, which leads to severe variation in the heat transfer coefficient, and an increase in Nusselt number.

4.2. Effect of shape factor and Rayleigh number

Figure 4 shows the local Nusselt number for two hot walls, AB and BC, for Rayleigh numbers $10, 10^3, 10^4$ and 10^5, and shape factors $2W/L = 1, 0.8$ and 0.6. For low Rayleigh numbers (Ra $= 10$ and Ra $= 10^3$), the value of the local Nusselt number is symmetrical, with respect to point B. As shown in Figure 4, the higher Nusselt number occurs at lower shape factors. At Ra $= 10^4$, the value of the Nusselt number at the vertical wall increases until it reaches its maximum value in middle of this wall. After that, it begins to decrease and reaches its minimum value at point B. It is notable that at the same Rayleigh number, the local Nusselt number along the horizontal hot wall increases and reaches maximum value before the middle point of the wall. After that, for shape factors $2W/L = 0.8$ and 1, the local Nusselt number decreases. For $2W/L = 0.6$, the local Nusselt number leads to a constant value at point C. At Ra $= 10^5$, there is a maximum value for the Nusselt number at the vertical hot wall. However, at the horizontal wall, this maximum value occurs at different shape factors and positions, and the Nusselt number will further increase, with respect to the vertical wall. It is notable that at $2W/L = 0.6$, for the horizontal wall, there are two maximum points for the Nusselt number. It is due to the existence of two rotating vortexes in the horizontal port of the cavity that was mentioned earlier.

4.3. The average Nusselt number

Figure 5 shows the average Nusselt number as a function of Rayleigh number for shape factors $2W/A = 0.6, 0.8$ and 1 at $\varphi = 0$ and 0.05. As shown in Figure 5, the variations of average Nusselt number can be divided into two parts. In the first part, the value of the Nusselt number is constant for every shape factor and does not change with Rayleigh number. This part shows pure conduction. In the second part, the value of the Nusselt number changes linearly (in the diagram it is shown in its logarithmic form) and the slope of these lines are dependent on shape factor. This part represents natural convection. It is notable that a decrease in shape factor leads to an increase in average Nusselt number. At shape factor $2W/L = 1.0$, for Ra$\leq 3 \times 10^3$, the average Nusselt number is constant, and, after this Ra value, it increases. However, in the case of shape factor $2W/L = 0.8$, the increase in average Nusselt number begins from Ra $= 8 \times 10^3$. Likewise, in the case of shape factor $2W/L = 0.6$, this increase begins from Ra $= 2 \times 10^4$. In this state, the obtained values are more remarkable, with respect to the two previous states.

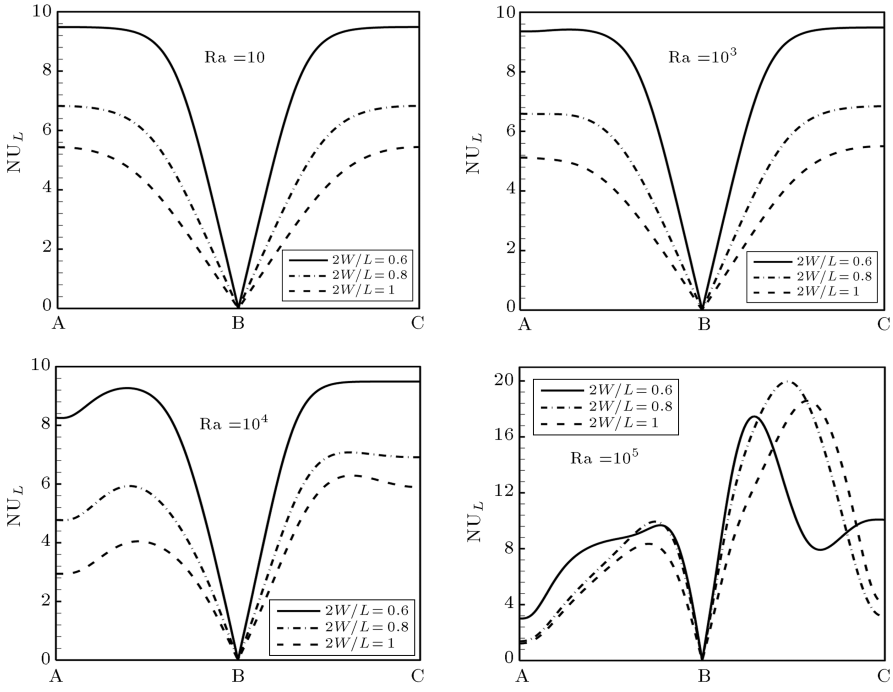

Figure 4. Local Nusselt number for Ra $= 10, 10^3, 10^4$ and 10^5 and shape factors $2W/A = 0.6$, 0.8 and 1 at $\varphi = 0.0$

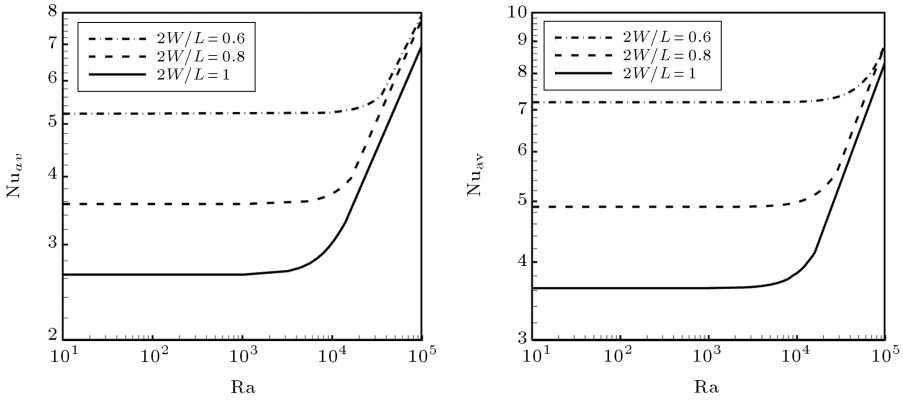

Figure 5. Variation of average Nusselt number for different Rayleigh numbers and shape factors (the left diagram is related to $\varphi = 0$ and the right diagram is related to $\varphi = 0.05$).

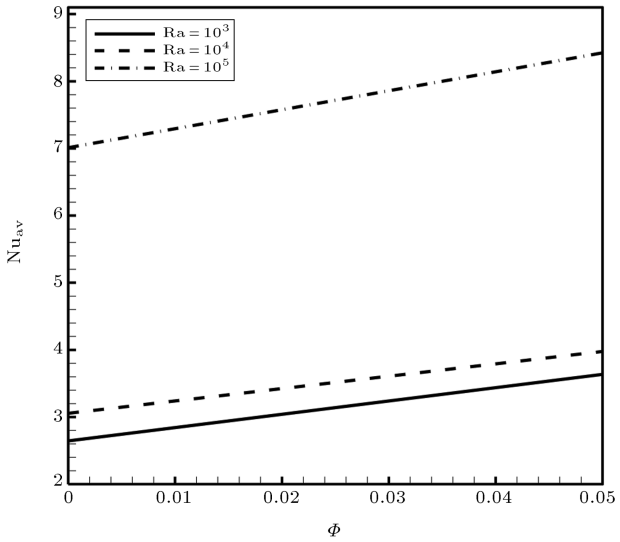

Figure 6. The average Nusselt number for Ra $= 10^3, 10^4$ and 10^5 for solid volume fraction in range $\varphi = 0 - 0.05$.

4.4. Solid volume fraction effect on Nusselt number

Figure 6 shows the average Nusselt number as a function of the solid volume fraction in the range of 0-0.05 for Rayleigh numbers $10^3, 10^4$ and 10^5. As shown in Figure 6, for all Rayleigh numbers, an increase in the solid volume fraction leads to a rise in the Nusselt number value, which is an expected result. This noticeable increase was about 25%-30%. It is of note that the variation of Nusselt number at different Rayleigh numbers is linear and changes with the solid volume fraction. This linear behavior is due to the linear variation of the thermal conductivity of nanofluid.

4.5. Inclination angle effect on Nusselt number

Figure 7 shows the stream lines and isotherm lines for Rayleigh numbers, 10^4 and 10^5, for solid volume fraction, $\varphi = 0.05$, with shape factor, $2W/L = 1$,

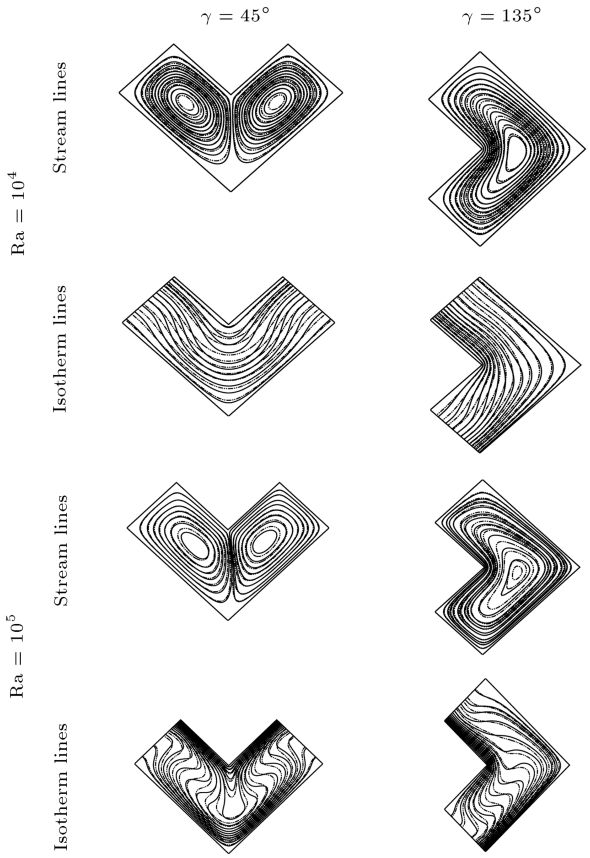

Figure 7. Stream lines and isotherm lines for Rayleigh numbers Ra $= 10^4$ and 10^5 for solid volume fraction $\varphi = 0.05$ with shape factor $2W/L = 1$ and inclination angles $\gamma = 45°$ and 135°.

and inclination angles, $\gamma = 45°$ and 135°. As shown in Figure 7, at the mentioned Rayleigh numbers for inclination angle $\gamma = 45°$, two CW rotating vortexes are formed in the flow field, whereas at inclination angle $\gamma = 135°$, there is just one CW rotating vortex. These variations are evident in isotherm lines.

Figure 8 shows the variation of average Nusselt number as a function of inclination angles (γ) for

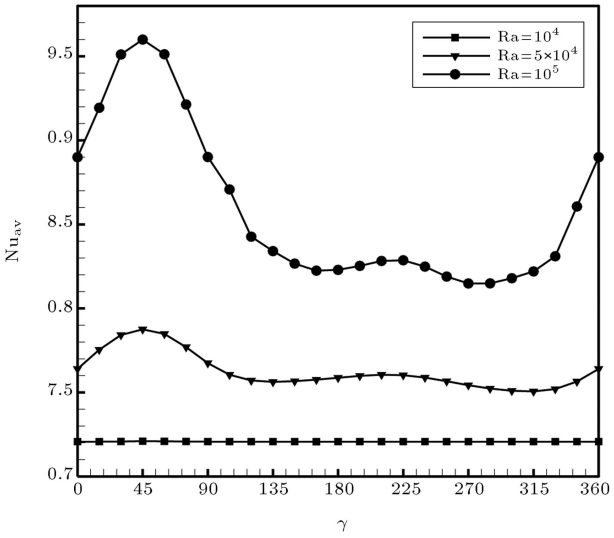

Figure 8. The average Nusselt number at different Rayleigh numbers for $\varphi = 0.05$.

different Rayleigh numbers at the solid volume fraction, $\varphi = 0.05$. For low Rayleigh numbers ($Ra \leq 10^4$), the variation of Nusselt number, with respect to the inclination angle, is negligible, which means that for low Rayleigh numbers, the conduction heat transfer predominates. For Rayleigh numbers, 5×10^4 and 10^5, the variation of average Nusselt number is dependent on the shape factor. The variation of Nusselt number, with respect to inclination angle (γ) at Rayleigh number $Ra = 5 \times 10^4$, is similar to 10^5. As was shown in Figure 8, the maximum heat transfer occurs at inclination angle $\gamma = 45°$ and in the convection region. There is an interesting phenomenon, where the minimum average Nusselt number is seen at two inclination angles ($\gamma = 160°$ and $\gamma = 292°$).

The diagram of Nusselt number variations, with respect to the inclination angle, has two symmetrical regions in the convection region. One symmetrical region is located at an inclination angle in the range $0° \leq \gamma \leq 90°$, and the second symmetrical region is located in the range $90° \leq \gamma \leq 360°$

As mentioned earlier, in the investigation, the shape factor is defined as $2W/L$. Figrue 9 presents the average Nusselt number as a function of $2W/L$ for Rayleigh numbers $10^4, 10^5$, and inclination angles, $\gamma = 0°$ and $45°$. For low shape factors ($2W/L \leq 0.3$), the Nusselt number variation for both Rayleigh number and inclination angle is the same. In addition, at these shape factors ($2W/L \leq 0.3$), the effect of Rayleigh number on Nusselt number is negligible. At Rayleigh number equal to 10^4, and for both inclination angles $\gamma = 0°$ and $45°$, by an increase in shape factor, the average Nusselt number decreases, whereas, at Rayleigh number equal to 10^5, for shape factors above $2W/L = 0.4$, the average Nusselt number is constant and presents small fluctuations.

5. Conclusion

In this work, nanofluid natural convection in an inclined L-shape cavity has been studied. The effects of shape factor and inclination angle for different Rayleigh numbers on average Nusselt number were examined. It is found that for low Rayleigh numbers, the Nusselt number is constant. In other words, at low Rayleigh numbers, the average Nusselt number has no dependence on Rayleigh number. When the shape factor decreases, the average Nusselt number increases and, at different shape factors, the Nusselt number changes linearly. Moreover, the results show that an increase in solid volume fraction leads to an increase in average Nusselt number value and these variations are linear. It is notable that at solid volume fraction $\varphi = 0.05$, for all Rayleigh numbers, the Nusselt number increases about 30%, with respect to pure fluid. At high Rayleigh numbers, where the convection heat transfer is predominated on conduction heat transfer, the Nusselt number has a maximum value at $\gamma = 45°$ and two minimum values at $\gamma = 160°$ and $292°$. Also, the diagram of Nusselt number variations, with respect to inclination angle, has two symmetrical regions in the convection region. One symmetrical region is located at an inclination angle in the range $0° \leq \gamma \leq 90°$ and the second symmetrical region is located in the

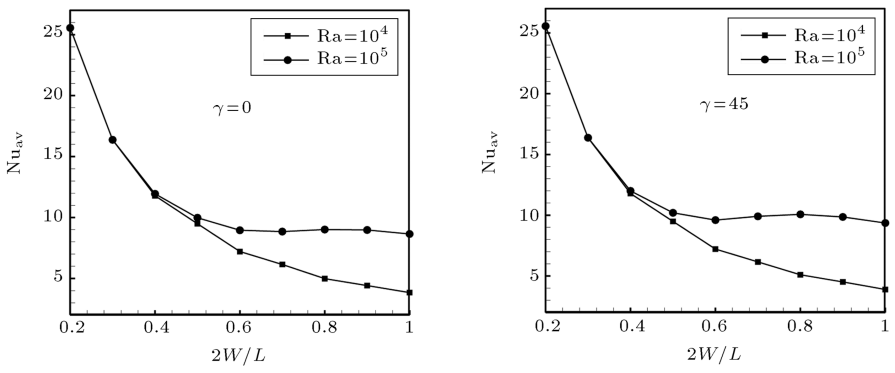

Figure 9. Average Nusselt number at Rayleigh number 10^4 and 10^5 for $\varphi = 0.05$ at shape factors $2W/L = 0.2 - 1$.

range $90° \leq \gamma \leq 360°$. Finally, it can be said that an increase in solid volume fraction leads to a rise in average Nusselt number value, and at inclination angle $\gamma = 45°$, the average Nusselt number presents a maximum value.

Nomenclature

A	Heat transfer area, m^2
c_p	Specific heat, $Jkg^{-1}K^{-1}$
g	Gravitational acceleration, ms^{-2}
h	Heat transfer coefficient, Wm^{-2} K^{-1}
L	Length of walls, m
k	Thermal conductivity, $Wm^{-1}K^{-1}$
Nu	Nusselt number
Nu_{ave}	Average Nusselt number
n	Unit normal vector
p	Pressure, Nm^{-2}
P	Dimensionless pressure
Pr	Prandtl number
q	Heat flux, Wm^{-2}
Ra	Rayleigh number
S	Surface, m^2
T	Dimensional temperature, K
T_c	Temperature of cold wall, K
T_h	Temperature of hot wall, K
u, v	Dimensional velocity components in x and y directions, ms^{-1}
U, V	Dimensionless velocity components in X and Y directions
x, y	Dimensional Cartesian coordinates, m
X, Y	Dimensionless Cartesian coordinates

Greek symbols

α	Thermal diffusivity, m^2s
β	Thermal expansion coefficient, K^{-1}
γ	Inclination angle
θ	Dimensionless temperature
μ	Dynamic viscosity, $kgm^{-1}s$
ν	Kinematic viscosity, m^2s
ρ	Density, kgm^{-3}
φ	Volume fraction of the nanoparticles

Subscripts

ave	Average
eff	Effective
c	Cold
f	Fluid
nf	Nanofluid
p	Particle
s	Solid particles
w	Wall

References

1. Chen, C.L. and Cheng, C.H. "Buoyancy-induced flow and convective heat transfer inside an inclined arc-shaped enclosure", *Int. J. Heat and Fluid Flow*, **23**, pp. 823-830 (2002).
2. Mahmud, S., Das, P.K., Hyder, N. and Islam, A.K.M. "Free convection in an enclosure with vertical wavy walls", *Int. J. Therm. Sci.*, **41**, pp. 440-446 (2002).
3. Lee, J.H., Back, Y.R., Lee, S.R. and Faghri, M. "Natural convection in enclosures with an irregular wall", *Transport Phenomena in Heat and Mass Transfer*, pp. 112-123 (1992).
4. Cheng, C.H. and Chao, C.C. "Numerical prediction of the buoyancy driven flow in the annulus between horizontal eccentric elliptical cylinders", *Numerical Heat Transfer (A)*, **30**, pp. 283-303 (1996).
5. Tansim, S.H. and Mahmud, S. "Laminar free convection inside an inclined L-shaped enclosure", *Int. Commun. Heat and Mass Transfer*, **33**, pp. 936-942 (2006).
6. Eastman, J.A., Choi, S.U.S., Li, S., Yu, W. and Thompson, L.J. "Anomalously increased effective thermal conductivities of ethylene glycol-based nanofluids containing copper nanoparticles", *Appl. Phys. Lett.*, **78**, pp. 718-720 (2001).
7. Xie, H.Q., Lee, H., Youn, W. and Choi, M. "Nanofluids containing multiwalled carbon nanotubes and their enhanced thermal conductivities", *J. Appl. Phys.*, **94**(8), pp. 4967-4971 (2003).
8. Jana, S., Khojin, A.S., Zhong, W.H. "Enhancement of fluid thermal conductivity by the addition of single and hybrid nano-additives", *Thermochimica Acta*, **462** (1-2), pp. 45-55 (2007).
9. Choi, S.U.S. "Enhancing thermal conductivity of fluids with nanoparticles", *Developments and Applications of Non-Newtonian Flows*, *ASME*, **231**(66), New York, pp. 99-105 (1995).
10. Shahi, M., Mahmoudi, A.H. and Talebi, F. "Numerical study of mixed convective cooling in a square cavity ventilated and partially heated from the below utilizing nanofluid", *Int. Commun. Heat and Mass Transfer*, **37**, pp. 201-213 (2010).
11. Santra, A.K., Sen, S. and Chakraborty, N. "Study of heat transfer augmentation in a differentially heated square cavity using copper-water nanofluid", *Int. J. Therm. Sci.*, **47**, pp. 1113-1122 (2008).
12. Patel, H.E., Pradeep, T., Sundararajan, T., Dasgupta, A., Dasgupta, N. and Das, S.K. "A micro convectionmodel for thermal conductivity of nanofluid", *Pramana-Journal of Physics*, **65**, pp. 863-869 (2005).

13. Brinkman, H.C. "The viscosity of concentrated suspensions and solutions", *J. Chem. Phys.*, **20**, pp. 571-581 (1952).
14. Patnkar, S.V. *Numerical Heat Transfer and Fluid Flow*, Hemisphere, New York (1980).
15. Mahmud, S. "Free convection inside an L-shaped enclosure", *Int. Commun. Heat and Mess Transfer*, **29**, pp. 1005-1013 (2002).

Biographies

Ali Akbar Abbasian Arani received BS and MS degrees from Sharif University of Technology, Tehran, Iran, in 1991 and 1994, respectively, and his PhD degree from the University of Bordeaux 1, France, in 2006. He is currently Associate Professor in the Mechanical Engineering Department at the University of Kashan, Iran. His research interests include fluid mechanics and heat transfer, nanofluids and energy conversion.

Alizamen Maghsoudi received BS and MS degrees from the University of Kashan, Iran, in 2001 and 2011, respectively. His research interests include convection heat transfer, nanofluids and energy conversion.

Amirhossein Niroumand received a BS degree from the Islamic Azad University, Khomeinishahr, Iran, in 2008, and his MS degree, in 2011, from the University of Kashan, Iran, where he is currently a PhD degree student. His research interests include nanofluid, convection heat transfer and microchannels.

Syeed Mohammad Ebrahim Derakhshani received his BS degree from Ferdowsi University, Mashad, Iran, in 2002, and his MS degree from Iran University of Science and Technology, Tehran, Iran, in 2007. He is currently a PhD degree student at Delft University of Technology, the Netherlands. His research interests include artificial neural networks, nanofluid and computational fluid dynamics.